Task-Centric Policy Optimization from Misaligned Motion Priors

Ziang Zheng [*1] **Kai Feng** [*2] **Yi Nie** [3] **Shentao Qin** [1]

Abstract

Humanoid control often leverages motion priors from human demonstrations to encourage natural behaviors. However, such demonstrations are frequently suboptimal or misaligned with robotic tasks due to embodiment differences, retargeting errors, and task-irrelevant variations, causing naïve imitation to degrade task performance. Conversely, task-only reinforcement learning admits many task-optimal solutions, often resulting in unnatural or unstable motions. This exposes a fundamental limitation of linear reward mixing in adversarial imitation learning. We propose *Task-Centric Motion Priors* (TCMP), a task-priority adversarial imitation framework that treats imitation as a conditional regularizer rather than a co-equal objective. TCMP maximizes task improvement while incorporating imitation signals only when they are compatible with task progress, yielding an adaptive, geometry-aware update that preserves task-feasible descent and suppresses harmful imitation under misalignment. We provide theoretical analysis of gradient conflict and task-priority stationary points, and validate our claims through humanoid control experiments demonstrating robust task performance with consistent motion style under noisy demonstrations.

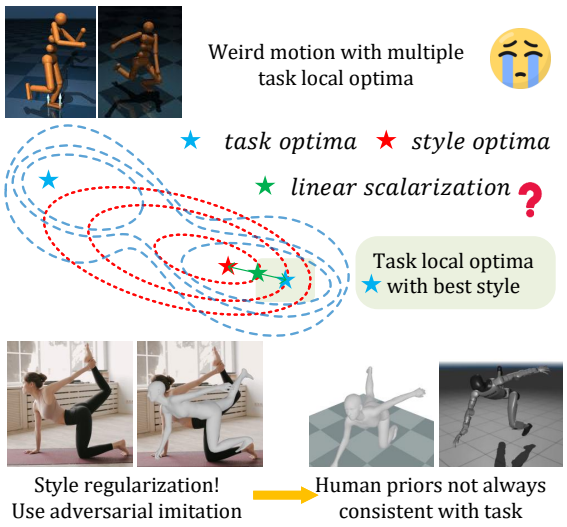

Figure 1. Task-only optimization yields unnatural behaviors, while motion priors may be misaligned. We resolve this by selecting the best style among task-optimal solutions.

1. Introduction

Humanoid robots offer a unique advantage among robotic platforms: their morphology enables the direct reuse of rich human motion knowledge. At the same time, humanoid control remains notoriously difficult due to high-dimensional dynamics, frequent contacts, and the complexity of task design. Pure reinforcement learning with hand-crafted rewards often leads to abnormal postures or unstable behaviors, while designing rewards that simultaneously enforce task completion and natural motion is highly non-trivial and lacks principled guidance (Heess et al., 2017; Hwangbo et al., 2019; Lillicrap et al., 2016; Todorov et al., 2012; Zheng et al., 2025a).

To address these challenges, human motion priors have become a central tool in humanoid learning (Zhan et al., 2025; Merel et al., 2018; Lee et al., 2020). In practice, two dominant paradigms are commonly adopted. The first is motion tracking (Peng et al., 2018), where a low-level controller is trained to follow reference trajectories and task execution is delegated to a higher-level planner. The second is adversarial imitation learning (Ho & Ermon, 2016; Peng et al., 2021), which preserves the reinforcement learning formulation while encouraging the policy to match the distribution of expert motions during task optimization.

Both approaches, however, rely on a strong assumption: that the reference motions are of high quality and well aligned with the robot's task and embodiment. In real robotic settings, this assumption is rarely satisfied (Le et al., 2018; Wu et al., 2019; Peng et al., 2020). Human motion data is typically obtained from motion capture systems or reconstructed

[*]Equal contribution [1]School of Vehicle and Mobility, Tsinghua University, Beijing, China [2]International School, Beijing University of Post and, Beijing, China [3]The Department of Automation, Tsinghua University, Beijing, China. Correspondence to: Ziang Zheng <zhengza24@mails.tsinghua.edu.cn>.

Preprint. January 28, 2026.

from videos, and then retargeted to the robot. Differences in morphology (Zheng et al., 2025b), sensing noise, and retargeting errors often require complex post-processing. More importantly, human motions naturally contain substantial task-irrelevant behaviors and stylistic variations that are not optimal for the robotic task.

As a result, directly incorporating imitation objectives into task optimization can distort the original task objective (Sener & Koltun, 2018; Fliege & Svaiter, 2000). A common empirical symptom is that policies trained with strong imitation signals exhibit severe oscillations or jitter, requiring additional reward shaping such as increasing action penalties to recover task stability.

Fig. 1 illustrates this dilemma. Naïve linear reward mixing fails to resolve the tension, often sacrificing task optimality in favor of imitation. We address this by formulating the integration of motion priors as a task-priority first-order constraint optimization problem, where task improvement is always enforced and imitation is incorporated only when locally compatible (Boyd & Vandenberghe, 2004). This yields a gradient-level integration scheme that preserves task optimality while leveraging motion priors to resolve stylistic ambiguity.

In summary, this paper makes the following contributions:

- We identify a fundamental failure mode of adversarial imitation learning in robotic control, where linear reward mixing induces gradient conflict under demonstration misalignment, leading to degraded task performance or unstable behaviors.
- We formulate *Task-Centric Motion Priors* (TCMP), a task-priority framework that integrates motion imitation through first-order constrained optimization, enabling gradient-level fusion that preserves task-optimality while selecting stylistically preferred solutions.

2. Preliminary

2.1. Reinforcement Learning

We consider episodic reinforcement learning in a Markov Decision Process (MDP) $(\mathcal{S}, \mathcal{A}, P, r_{\text{task}}, \gamma)$. A stochastic policy $\pi_\theta(a \mid s)$ induces trajectories $\tau = (s_0, a_0, \ldots, s_T)$ and is trained to maximize the expected discounted return (Sutton et al., 2000)

$$J_{\text{task}}(\pi_\theta) = \mathbb{E}_{\tau\sim\pi_\theta}\left[\sum_{t=0}^{T}\gamma^t r_{\text{task}}(s_t, a_t)\right]. \tag{1}$$

Proximal Policy Optimization (PPO) (Schulman et al., 2017b) is a widely used algorithm which maximizes the clipped surrogate objective

$$\mathcal{L}_{\text{PPO}}(\theta) = \mathbb{E}_t\Big[\min\big(r_t(\theta)\hat{A}_t,\ \text{clip}(r_t(\theta), 1-\epsilon, 1+\epsilon)\hat{A}_t\big)\Big], \tag{2}$$

where $r_t(\theta) = \pi_\theta(a_t \mid s_t)/\pi_{\theta_{\text{old}}}(a_t \mid s_t)$ and $\hat{A}_t$ denotes an advantage estimate (Schulman et al., 2015):

$$\hat{A}_t = \sum_{l=0}^{\infty}(\gamma\lambda)^l\big(r(s_{t+l}, a_{t+l}) + \gamma V_\psi(s_{t+l+1}) - V_\psi(s_{t+l})\big). \tag{3}$$

2.2. Adversarial Imitation Learning

Adversarial imitation learning methods aim to align the occupancy measure of a learned policy with that of expert demonstrations (Ho & Ermon, 2016; Ziebart et al., 2008; Finn et al., 2016).

In humanoid motion imitation, expert demonstrations are typically provided as motion capture sequences (Liao et al., 2025), optionally retargeted to the robot morphology (Ze et al., 2025), and do not contain actions or rewards (Torabi et al., 2018). AMP addresses this setting by defining the discriminator over partial state transitions $(s_t^{\text{kine}}, s_{t+1}^{\text{kine}})$, where $s^{\text{kine}} \subset s$ consists of kinematic features such as joint positions and joint velocities.

Let $D_\phi(s_t^{\text{kine}}, s_{t+1}^{\text{kine}})$ denote the AMP discriminator. The imitation reward is defined as

$$r_{\text{style}}(s_t, s_{t+1}) = \frac{1}{2}\left(1 + \sigma\big(D_\phi(s_t^{\text{kine}}, s_{t+1}^{\text{kine}})\big)\right), \tag{4}$$

where $\sigma(\cdot)$ is the sigmoid function.

Given policy-generated transitions (s_t, s_{t+1}) and demonstration transitions $(\tilde{s}_t, \tilde{s}_{t+1})$ sampled from the demonstration buffer $\mathcal{B}_{\text{demo}}$, the discriminator objective is

$$\begin{aligned}\mathcal{L}_D(\phi) = {} & \mathbb{E}_{(s_t, s_{t+1})\sim\pi_\theta}\left[\big(D_\phi(s_t^{\text{kine}}, s_{t+1}^{\text{kine}}) - 1\big)^2\right] \\ & + \mathbb{E}_{(\tilde{s}_t, \tilde{s}_{t+1})\sim\mathcal{B}_{\text{demo}}}\left[\big(D_\phi(\tilde{s}_t^{\text{kine}}, \tilde{s}_{t+1}^{\text{kine}})\big)^2\right] + \lambda_{\text{gp}}\,\mathcal{L}_{\text{GP}},\end{aligned} \tag{5}$$

where $\mathcal{L}_{\text{GP}}$ denotes a gradient penalty regularizer.

Standard AMP-based methods optimize a joint objective

$$J_\lambda(\pi) = \lambda J_{\text{task}}(\pi) + (1-\lambda)J_{\text{style}}(\pi), \tag{6}$$

with a manually tuned coefficient λ balancing task performance and imitation (Parisi et al., 2014; Yu et al., 2020). This fixed weighting motivates our task-centric reformulation introduced in the next section.

3. Method

In this section, we present **TCMP** (Task-Centric Motion Priors), a policy optimization framework that leverages adversarial imitation signals as auxiliary guidance, rather than

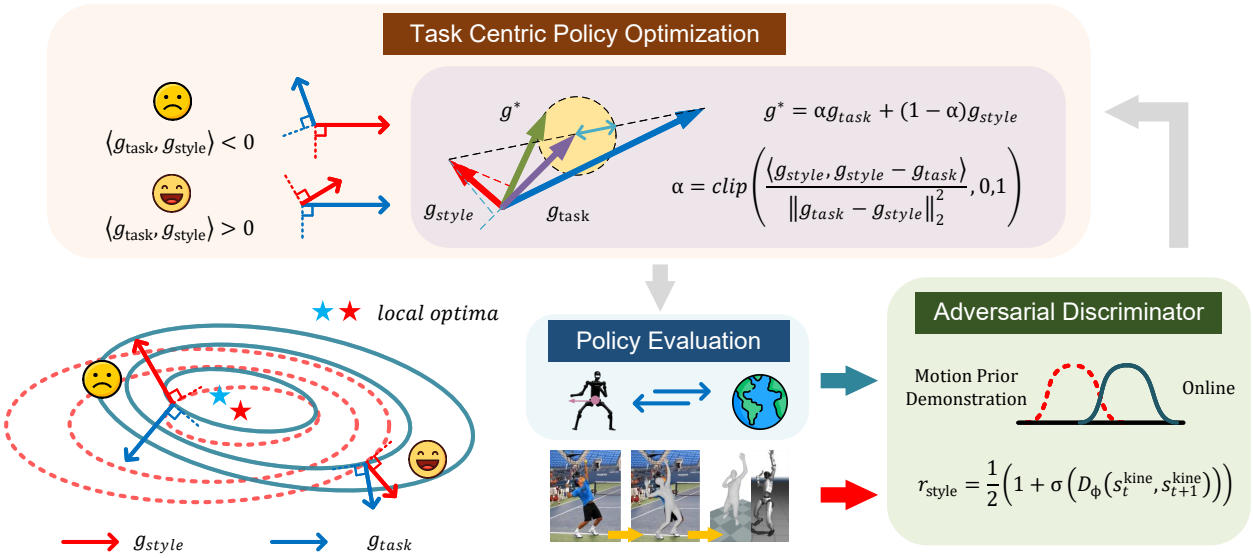

Figure 2. **Framework of TCMP.** Instead of linearly combining task and imitation rewards, TCMP treats adversarial imitation as a conditional regularizer guided by optimization geometry. At each update, the policy is optimized primarily for task performance, while imitation gradients are adaptively incorporated only when they do not interfere with task improvement.

primary optimization objectives. The overall framework is illustrated in Fig. 2.

3.1. Adversarial Imitation as a Noisy Optimization Signal

A common practice in imitation-augmented reinforcement learning is to combine task and imitation signals at the reward level, yielding the scalarized objective in Eq. (6).

Definition 3.1 (Gradient Conflict)**.** Two objectives J_{task} and J_{style} are said to be *locally conflicting* at parameters θ if

$$\langle g_{\text{task}}, g_{\text{style}} \rangle < 0. \tag{7}$$

Lemma 3.2 (Gradient Decomposition under Linear Scalarization)**.** *The policy gradient of the scalarized objective in Eq. (6) decomposes as*

$$\nabla_\theta J_\lambda(\pi_\theta) = \lambda g_{task} + (1-\lambda) g_{style}, \tag{8}$$

where $g_{task} = \nabla_\theta J_{task}(\pi_\theta)$ *and* $g_{style} = \nabla_\theta J_{style}(\pi_\theta)$.

Proof. This follows directly from the linearity of differentiation. See Appendix A.1. □

To analyze the local effect of such scalarization, we adopt a first-order view of policy optimization.

Lemma 3.3 (First-Order Objective Variation)**.** *For a sufficiently small step size* $\eta > 0$*, the first-order change of* J_i *under the update* $\theta' = \theta + \eta h$ *satisfies*

$$J_i(\theta') - J_i(\theta) = \eta \langle \nabla_\theta J_i(\theta), h \rangle + o(\eta). \tag{9}$$

Proof. See Appendix A.2. □

By Def. 3.1 and Lemma 3.3, a negative inner product implies that increasing the influence of imitation induces a first-order degradation of task performance, a phenomenon commonly referred to as gradient interference in multi-task learning (Yu et al., 2020).

Definition 3.4 (Task-optimal policy set)**.** Let $J_{\text{task}}(\pi)$ denote the expected return induced by the task reward. We define the set of task-optimal policies as

$$\Pi^\star_{\text{task}} \triangleq \left\{ \pi \;\middle|\; J_{\text{task}}(\pi) = \sup_{\pi'} J_{\text{task}}(\pi') \right\}. \tag{10}$$

Proposition 3.5 (Imitation distinguishes task-equivalent policies)**.** *Assume that* $J_{style}(\pi)$ *depends on the occupancy measure* ρ_π*. If there exist* $\pi_1, \pi_2 \in \Pi^\star_{task}$ *such that* $\rho_{\pi_1} \neq \rho_{\pi_2}$*, then*

$$J_{style}(\pi_1) \neq J_{style}(\pi_2). \tag{11}$$

Proof. See Appendix A.3. □

Proposition 3.5 shows that adversarial imitation does not refine the task objective itself, but instead imposes a preference over policies that are indistinguishable under J_{task}.

Assumption 3.6 (Demonstration misalignment)**.** There exists $\delta > 0$ such that, for all $\pi \in \Pi^\star_{\text{task}}$,

$$D(\rho_\pi \,\|\, \rho_E) \geq \delta, \tag{12}$$

where $D(\cdot \,\|\, \cdot)$ denotes the divergence induced by the adversarial discriminator.

Theorem 3.7 (Failure of linear scalarization under misalignment)**.** *Under Assumption 3.6, for any fixed $\lambda \in (0,1)$, every maximizer of the scalarized objective*

$$J_\lambda(\pi) \triangleq \lambda J_{task}(\pi) + (1-\lambda) J_{style}(\pi) \tag{13}$$

does not belong to $\Pi^\star_{task}$.

Proof. See Appendix A.4. □

Theorem 3.7 implies that, when demonstrations are misaligned with the task objective, linear reward scalarization necessarily admits optimization directions that deviate from task-optimality.

3.2. Task-Centric Gradient Projection

Motivated by the analysis in Sec. 3.1, we seek an update direction that prioritizes task improvement while ensuring that imitation does not actively oppose the update. Rather than treating imitation as a co-equal objective, we impose it as a first-order feasibility constraint, following classical gradient projection methods in constrained optimization (Chaudhry et al., 2019; Yu et al., 2020; Sener & Koltun, 2018).

At each iteration, given the task and imitation gradients g_{task} and g_{style}, we solve the following constrained optimization problem:

$$\begin{aligned} \max_{\Delta\theta} \quad & \langle g_{\text{style}}, \Delta\theta \rangle \\ \text{s.t.} \quad & \langle g_{\text{task}}, \Delta\theta \rangle \geq 0, \\ & \|\Delta\theta\|_2 \leq \epsilon. \end{aligned} \tag{14}$$

The constraint $\langle g_{\text{task}}, \Delta\theta \rangle \geq 0$ ensures that the update does not decrease the task objective to first order (cf. Lemma 3.3), while the norm constraint prevents arbitrarily large steps.

Proposition 3.8 (Closed-form solution)**.** *Problem (14) admits a closed-form solution. The optimal update direction can be written as*

$$\Delta\theta^\star = \epsilon \frac{g^\star}{\|g^\star\|_2}, \qquad g^\star = \alpha g_{task} + (1-\alpha) g_{style}, \tag{15}$$

where the mixing coefficient $\alpha \in [0,1]$ is given by

$$\alpha = \text{clip}\left(\frac{\langle g_{style},\, g_{style} - g_{task} \rangle}{\|g_{task} - g_{style}\|_2^2},\; 0,\; 1 \right). \tag{16}$$

Proof. See Appendix A.5. □

Importantly, α is not a hyperparameter but a function of the local gradient geometry. When g_{task} and g_{style} are aligned, the task-feasibility constraint is typically inactive, and $\alpha \approx 0$, allowing imitation gradients to assist task learning. When the two gradients conflict, the constraint becomes active, and α increases to ensure task-feasible updates, effectively projecting the update onto the feasible half-space.

Algorithm 1 Task-Centric Motion Priors

Require: demonstrations $\mathcal{B}_{\text{demo}} = \{(s_t^{\text{kine}}, s_{t+1}^{\text{kine}})\}$; policy π_θ; value function V_ψ; discriminator D_ϕ

for iteration $k = 1, 2, \ldots$ **do**
  Collect data and estimate advantage:
    $\tau = \{(s_t, a_t, s_{t+1})\}_{t=0}^{T-1}$ with π_θ
    $\hat{r}_t^{\text{style}} \leftarrow r_{\text{style}}(s_t, s_{t+1})$ Eq. (4)
    Compute $\hat{A}^{\text{task}}$ and $\hat{A}_t^{\text{style}}$ Eq. (3)
  Task-centric policy optimization:
    $L_{\text{task}}(\theta) \leftarrow \mathbb{E}_t\left[\mathcal{L}_{\text{PPO}}(\theta; \hat{A}_t^{\text{task}})\right]$ Eq. (2)
    $L_{\text{style}}(\theta) \leftarrow \mathbb{E}_t\left[\mathcal{L}_{\text{PPO}}(\theta; \hat{A}_t^{\text{style}})\right]$
    $g_{\text{task}} \leftarrow \nabla_\theta L_{\text{task}}(\theta),\ g_{\text{style}} \leftarrow \nabla_\theta L_{\text{style}}(\theta)$
    $\alpha \leftarrow$ closed form solution Eq. (16)
    $g \leftarrow \alpha g_{\text{task}} + (1-\alpha) g_{\text{style}}$ Eq. (15)
  Components update:
    $\theta \leftarrow \theta + \eta_\pi\, g$, $\psi \leftarrow \arg\min_\psi \mathbb{E}_t[(V_\psi(s_t) - \hat{V}_t)^2]$
    Sample $(s_t^{\text{kine}}, s_{t+1}^{\text{kine}}) \sim \tau$, $(\tilde{s_t^{\text{kine}}}, \tilde{s_{t+1}^{\text{kine}}}) \sim \mathcal{B}_{\text{demo}}$
    $\phi \leftarrow \arg\min_\phi \mathcal{L}_D(\phi)$ Eq. (5)
end for

Remark 3.9 (Optimality over linear scalarization). TCMP is fundamentally different from linear reward scalarization: it preserves task-optimality whenever possible and only invokes imitation to resolve ambiguity or conflict, rather than averaging objectives indiscriminately.

3.3. Practical Algorithm

We present a practical implementation of TCMP on top of PPO. The complete procedure is summarized in Alg. 1.

Data Collection and Advantage Estimation. We roll out the current policy π_θ to collect trajectories $\tau = \{(s_t, a_t, r_t^{\text{task}}, r_t^{\text{style}})\}_{t=0}^{T-1}$. Here, r_t^{task} denotes the task reward, while r_t^{style} is the adversarial imitation reward computed from the discriminator (Eq. 4). To separately estimate gradients for the two objectives, we compute two GAEs: (i) A_t^{task} using task rewards and value function V_{task}, (ii) A_t^{style} using adversarial rewards and value function V_{style}, both following the standard GAE formulation in Eq. 3.

Policy Optimization. Given the estimated gradients, we construct the task-centric update direction according to the gradient projection rule derived in Sec. 3.2. The resulting direction replaces the vanilla policy gradient inside the PPO clipped objective (Eq. 2).

Critic and Discriminator Updates. We update the task value function V_{task} and the adversarial value function V_{style} by minimizing the mean squared error between the value predictions and the target values computed via GAE (Eq. 3).

The discriminator is trained by Eq. 5.

3.4. Theoretical Analysis

Task-Feasible Descent Guarantee We begin by establishing that TCMP enforces task feasibility at the level of first-order policy updates, ensuring that adversarial imitation does not degrade task performance.

Assumption 3.10 (Lipschitz Continuity)**.** The task objective $J_{\text{task}}(\theta)$ and the style objective $J_{\text{style}}(\theta)$ are continuously differentiable, and their gradients are L-Lipschitz continuous, i.e.,

$$\|\nabla J_i(\theta_1) - \nabla J_i(\theta_2)\|_2 \le L\|\theta_1 - \theta_2\|_2, \quad \forall i \in \{\text{task}, \text{style}\}. \tag{17}$$

Definition 3.11 (Task-Feasible Direction)**.** A direction $h \in \mathbb{R}^d$ is said to be *task-feasible* at parameters θ if it satisfies

$$\langle g_{\text{task}}, h\rangle \ge 0, \tag{18}$$

where $g_{\text{task}} = \nabla_\theta J_{\text{task}}(\theta)$.

The following lemma characterizes the feasibility of the TCMP update direction.

Lemma 3.12 (Feasibility of Projected Update)**.** *Let g^* denote the TCMP update direction defined in Eq. (14). Then g^* is task-feasible, i.e.,*

$$\langle g_{task}, g^*\rangle \ge 0. \tag{19}$$

Proof. See Appendix A.6. □

We now state the main descent guarantee.

Theorem 3.13 (Task-Feasible Descent)**.** *Under Assumption 3.10, for a sufficiently small step size $\eta > 0$, the TCMP update $\theta' = \theta + \eta g^*$ satisfies*

$$J_{task}(\theta') \ge J_{task}(\theta) \tag{20}$$

up to first-order approximation.

Proof. Applying the first-order expansion in Lemma 3.3 completes the proof. See Appendix A.7. □

Stationary Point and Task-Priority Optimality We next characterize the limiting behavior of TCMP and formalize the notion of stationarity induced by task-priority optimization.

Definition 3.14 (Task-Priority Feasible Cone)**.** The task-feasible cone at parameters θ is defined as

$$\mathcal{C}_{\text{task}}(\theta) \triangleq \left\{h \in \mathbb{R}^d \;\middle|\; \langle g_{\text{task}}(\theta), h\rangle \ge 0\right\}. \tag{21}$$

This cone characterizes all first-order update directions that do not degrade the task objective.

Definition 3.15 (Task-Priority Stationary Point)**.** A parameter $\theta^\star$ is said to be *task-priority stationary* if there exists no direction $h \in \mathcal{C}_{\text{task}}(\theta^\star)$ such that

$$\langle g_{\text{task}}(\theta^\star), h\rangle > 0. \tag{22}$$

At such a point, no admissible first-order update can further improve the task objective while preserving task feasibility.

The following lemma provides a geometric characterization of task-priority stationarity.

Lemma 3.16 (Characterization of Task-Priority Stationarity)**.** *A parameter $\theta^\star$ is task-priority stationary if and only if either*

$$g_{task}(\theta^\star) = 0, \tag{23}$$

or

$$\langle g_{task}(\theta^\star), g_{style}(\theta^\star)\rangle \le 0, \tag{24}$$

and the TCMP update direction satisfies $g^*(\theta^\star) = 0$.

Proof. See Appendix A.8. □

We now relate this notion of stationarity to the asymptotic behavior of TCMP.

Theorem 3.17 (Limit Point Optimality of TCMP)**.** *Assume that the sequence of parameters $\{\theta_k\}$ generated by TCMP admits a limit point $\theta^\star$. Then $\theta^\star$ is task-priority stationary.*

Proof. See Appendix A.9. □

Convergence and Reduction Properties We finally discuss the convergence behavior of TCMP and its relationship to existing policy optimization methods.

Assumption 3.18 (Step Size and Boundedness)**.** The sequence of step sizes $\{\eta_k\}$ satisfies $\sum_k \eta_k = \infty$ and $\sum_k \eta_k^2 < \infty$. Furthermore, the gradients g_{task} and g_{style} are uniformly bounded.

Under standard assumptions for first-order policy optimization, we establish convergence of TCMP to a task-priority stationary point.

Theorem 3.19 (Convergence of TCMP)**.** *Under Assumptions 3.10 and 3.18, the sequence of parameters $\{\theta_k\}$ generated by TCMP converges to a task-priority stationary point as defined in Def. 3.15.*

Proof. See Appendix A.10. □

Proposition 3.20 (Reduction Property)**.** *TCMP reduces to direct optimization when the imitation gradient always conflicts with the task gradient. Conversely, TCMP recovers an adversarial imitation-style update direction.*

Proof. See Appendix A.11. □

Table 1. **Robustness to demonstration misalignment.** Performance comparison under varying degrees of misalignment between demonstrations and target tasks. We group tasks into aligned, mildly misaligned, and severely misaligned settings. Standard AMP-style reward mixing is sensitive to imitation strength and often degrades task return as misalignment increases. In contrast, **TCMP** maintains task-centric performance across all settings without per-task tuning, while still leveraging useful motion priors.

Task	Methods													
	PPO (task-only)		AMP (mid)				AMP (full)				TCMP (ours)			
	Ret.↑	Smooth.↑	Ret.↑	Smooth.↑	Style↑	Conv.↓	Ret.↑	Smooth.↑	Style↑	Conv.↓	Ret.↑	Smooth.↑	Style↑	Conv.↓
Aligned demonstrations														
Velocity(Natural)	293±13	-0.79±0.03	218±6	-1.01±0.04	108±6	1920	122±18	-4.87±0.44	120±15	800	320±5	-0.21±0.05	108±5	2000
Velocity(DogMove)	360±8	-0.75±0.02	305±7	-1.53±0.03	88±5	2260	57±22	-12.86±0.09	121±4	650	375±9	-0.14±0.04	76±7	2050
Mildly misaligned demonstrations														
Navigation(E2E)	8.7±0.5	-0.040±0.008	5.7±1.2	-0.018±0.010	143±12	550	-54±16	-3.0±1.2	120±18	540	11.8±0.1	-0.001±0.001	138±8	1100
Tracking	34±3	-0.021±0.009	22±2	-0.083±0.019	137±5	990	-28±9	-2.91±0.57	133±4	1390	33±3	-0.022±0.007	122±2	800
Punch(Hit-task)	23.1±0.5	-0.003±0.002	10.8±0.4	-0.68±0.16	150±3	1150	-62±3	-6.39±0.47	146±3	900	20.9±0.4	-0.003±0.002	129±2	1300
Severely misaligned demonstrations														
Punch(AMP-only)	18.7±1.0	-0.004±0.002	4.5±1.1	-0.97±0.05	128±12	880	-20±9	-2.52±0.12	123±13	860	17.1±2.1	-0.001±0.001	124±20	1500
Tracking(incl.PHC)	32±2	-0.024±0.03	20±3	-0.052±0.03	123±4	1100	-18±6	-2.3±0.8	139±4	900	31±2	-0.022±0.02	121±2	1500
Velocity(KneeWalk)	282±31	-0.81±0.10	268±4	-1.75±0.32	98±4	2000	91±13	-5.74±0.26	133±9	800	320±5	-0.39±0.27	96±4	2300

* ↑ (↓) indicates higher (lower) is better.
* Ret.: task return; Smooth.: motion smoothness; Style: AMP discriminator score.
* Conv.: environment steps to convergence.

Table 2. Task categories and demonstration alignment used in robustness evaluation.

Task Category	Align.	Imit. Role	#Tasks
Navigation (E2E)	Partial	Auxiliary	App.B.1
Punch (AMP-only)	Severe	Critical	App.B.2
Punch (Hit-task)	Partial	Critical	App.B.2
Tracking	Aligned	Critical	App.B.2
Tracking (incl. PHC)	Aligned	Critical	App.B.2
Velocity (Natural)	Aligned	Auxiliary	App.B.1
Velocity (DogMove)	Partial	Auxiliary	App.B.3
Velocity (KneeWalk)	Severe	Auxiliary	App.B.4

*Align. denotes task and demonstration alignment level, including Partial, Severe, Aligned. *Imit. Role denotes imitation importance in the task, where the Auxiliary means only influence the performance while the Critical implies that task cannot complete without imitation.

4. Experiments

As discussed in Sec. 3, TCMP treats imitation as a conditional regularizer rather than a primary optimization objective. Accordingly, our experiments are designed to answer the following questions:

- **Robustness to demonstration misalignment:** Can TCMP preserve task-centric performance when demonstrations are degraded, partially irrelevant, or misaligned with the task objective?
- **Optimization behavior under adversarial imitation:** How do imitation-induced gradients interact with task optimization during training, and can task-priority gradient projection prevent conflicting updates?
- **Role of adaptive weighting:** Can the influence of imitation be adaptively and *interpretable* regulated based on gradient geometry, rather than manual coefficient tuning?

These questions are addressed in Sec. 4.1, Sec. 4.2, and Sec. 4.3, respectively.

Experimental setup All experiments are conducted in IsaacLab (Makoviychuk et al., 2021), building on TrackerLab (Zheng, 2025a) and BeyondAMP (Zheng, 2025b). We consider eight humanoid control tasks instantiated on the Unitree G1 humanoid robot, all designed to be deployable on real hardware. Rather than assuming high-quality demonstrations, we explicitly stress-test learning under varying degrees of demonstration alignment, as summarized in Table 2. Detailed descriptions of dataset preprocessing, reward specifications, and task configurations are provided in App. B.

Evaluation metrics Policies are evaluated along three complementary dimensions aligned with the TCMP formulation: **task performance**, measured by task-specific returns or success rates; **motion quality**, captured by smoothness and stability-related metrics; and **style alignment**, quanti-

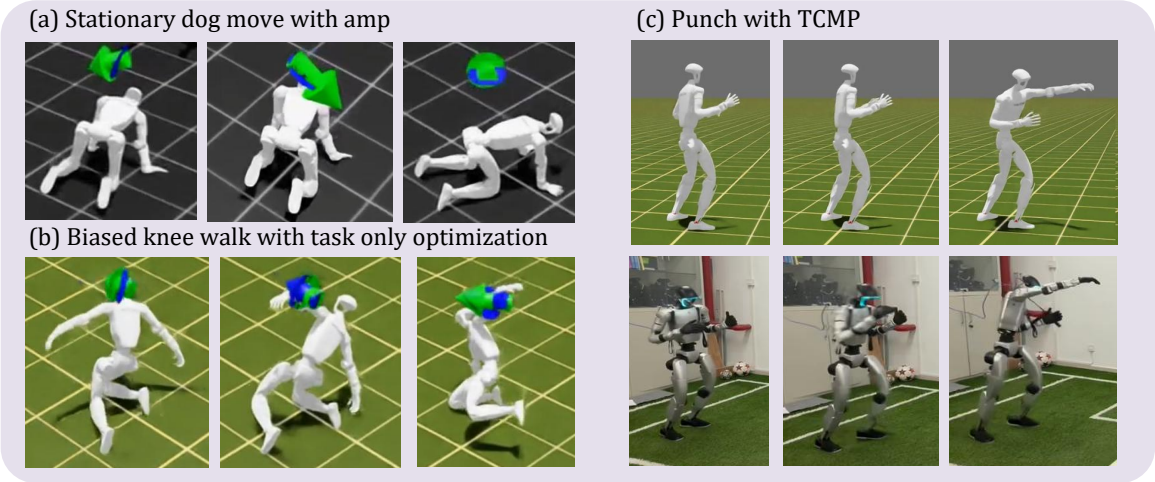

Figure 3. Qualitative comparison of optimization behaviors under demonstration misalignment. **Left:** Failure modes of AMP-style reward mixing under misaligned demonstrations, including imitation-dominated collapse (e.g., stationary dog-move) and task-only degeneration with physically implausible motions. **Right:** TCMP results on the same tasks, exhibiting task-centric, physically consistent behaviors in simulation and successful sim-to-real transfer on the Unitree G1 robot.

fied using discriminator-based scores or occupancy divergence relative to the demonstration distribution. Unless otherwise specified, all results are averaged over multiple random seeds.

4.1. Robustness to Demonstration Misalignment

We evaluate whether TCMP can maintain task-centric performance when demonstrations are degraded, irrelevant, or partially misaligned with the task objective. We compare TCMP with PPO (Schulman et al., 2017a) and AMP (Peng et al., 2021) under multiple imitation weight settings. Detailed hyperparameter configurations are provided in App. C.2.

Quantitative results Table 1 reports performance across the three evaluation dimensions. Across nearly all tasks with degraded or misaligned demonstrations, AMP exhibits a pronounced trade-off between task performance and style adherence, where increasing imitation weights often degrade task return. In contrast, TCMP consistently preserves task performance while retaining non-zero style alignment, without requiring manual coefficient tuning. Optional training curves (App. D.1) and radar visualizations (App. D.2) further highlight the balanced performance profile achieved by TCMP.

4.2. Optimization Behavior under Adversarial Imitation

We next analyze how task-priority optimization alters the training dynamics that commonly lead to failure modes in adversarial imitation.

Training dynamics under varying alignment Fig. 4 visualizes the evolution of the adaptive weighting α under aligned, partially aligned, and severely misaligned demonstrations. Under AMP-style reward mixing, task and imitation objectives remain entangled throughout training, causing policy updates to be dominated by discriminator-driven gradients once imitation rewards become strong. As a result, task performance often stagnates or degrades despite increasing imitation confidence.

In contrast, TCMP exhibits a qualitatively different optimization behavior. When demonstrations are well aligned with the task, α remains stable and close to zero, allowing imitation gradients to assist task learning. As alignment deteriorates, α increases progressively during training, selectively suppressing imitation updates that conflict with task improvement. Crucially, this transition emerges naturally from task-feasible gradient projection rather than a hand-designed schedule.

As a qualitative illustration of optimization behavior under demonstration misalignment, Fig. 3 compares the outcomes induced by reward-level imitation and TCMP. Under AMP-style reward mixing, imitation rewards can dominate policy updates, leading to characteristic failure modes such as imitation-dominated collapse or task-only degeneration with physically implausible motions. In contrast, TCMP enforces task-feasible updates and consistently yields task-centric, physically coherent behaviors, even when demonstrations conflict with the task objective.

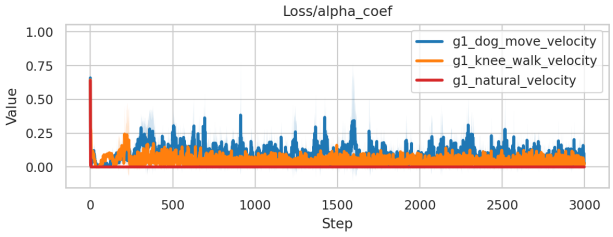

(a) Aligned demonstrations

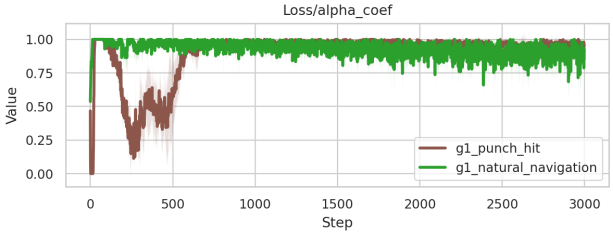

(b) Partially aligned demonstrations

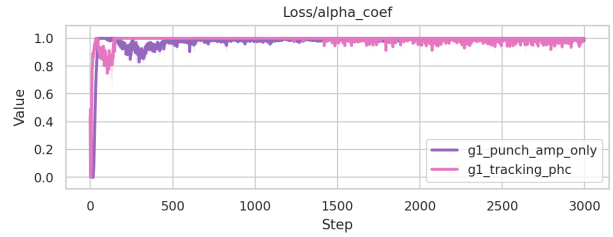

(c) Severely misaligned demonstrations

Figure 4. Evolution of the adaptive weighting α under different levels of demonstration alignment. When demonstrations are well aligned with the task, α remains stable and close to zero. As alignment degrades, α progressively increases, suppressing imitation updates that conflict with task-centric optimization.

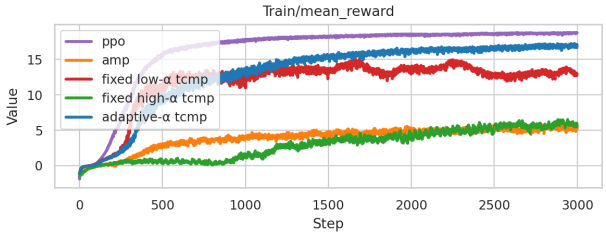

(a) Task reward

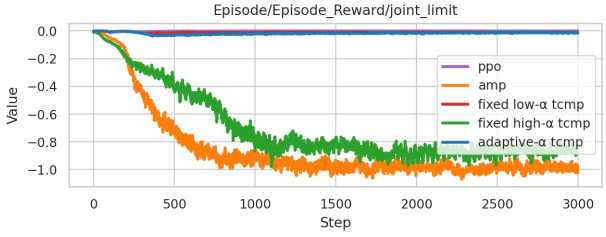

(b) Smoothness reward

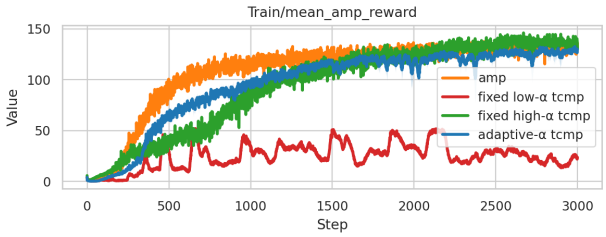

(c) Imitation (AMP) reward

Figure 5. Ablation study on the role of the adaptive weighting parameter α. We compare TCMP with adaptive α against fixed-α variants and AMP with matched reward-level mixing coefficients. Adaptive α enables TCMP to suppress misleading imitation gradients and recover task-centric optimization, while fixed-α methods collapse to AMP-like behavior under demonstration misalignment.

4.3. Role of Adaptive Weighting (α)

Fig. 5 compares TCMP with adaptive α against fixed-α variants and AMP baselines with matched reward coefficients. Across both aligned and partially aligned tasks, fixed-α TCMP degenerates toward reward-level mixing behavior: low α values degrade task performance, while large values collapse toward task-only optimization.

Takeaway Together, these results clarify that α in TCMP is not a hyperparameter controlling imitation strength, but an emergent quantity reflecting gradient compatibility. The advantage of TCMP arises not from careful tuning, but from enforcing task feasibility throughout training.

5. Conclusion

We introduced **Task-Centric Motion Priors (TCMP)**, a principled framework for integrating adversarial imitation into reinforcement learning under explicit task-priority constraints. By formulating imitation as a conditional regularizer enforced through task-feasible gradient projection, TCMP departs from reward-level scalarization and reveals a fundamental limitation of linear reward mixing: under demonstration misalignment, adversarial imitation can induce gradient conflicts that degrade task optimality.

Our analysis characterizes this conflict and leads to an adaptive weighting mechanism derived directly from gradient geometry. Across diverse humanoid locomotion and manipulation tasks with varying degrees of demonstration alignment, TCMP consistently preserves task performance while leveraging motion priors when beneficial. In contrast, AMP-style methods exhibit policy collapse and task degradation under misalignment, whereas TCMP maintains stable optimization behavior without manual coefficient tuning.

More broadly, TCMP provides an interpretable view of imitation in policy optimization, where the influence of demonstrations emerges from task feasibility rather than hyperparameter choice. We hope this task-centric perspective will inform future work on robust and transferable imitation-augmented reinforcement learning, especially in settings with imperfect or heterogeneous demonstrations.

References

Boyd, S. and Vandenberghe, L. Convex optimization. *Cambridge University Press*, 2004.

Chaudhry, A. et al. Efficient lifelong learning with gradient episodic memory. In *International Conference on Machine Learning*, 2019.

Finn, C., Levine, S., and Abbeel, P. Guided cost learning: Deep inverse optimal control via policy optimization. In *International Conference on Machine Learning*, 2016.

Fliege, J. and Svaiter, B. Steepest descent methods for multiobjective optimization. *Mathematical Methods of Operations Research*, 2000.

Heess, N., Tb, D., Sriram, S., Lemmon, J., Merel, J., Wayne, G., Tassa, Y., Erez, T., Wang, Z., Eslami, S., et al. Emergence of locomotion behaviours in rich environments. *arXiv preprint arXiv:1707.02286*, 2017.

Ho, J. and Ermon, S. Generative adversarial imitation learning. *Advances in neural information processing systems*, 29, 2016.

Hwangbo, J., Lee, J., Dosovitskiy, A., Bellicoso, D., Tsounis, V., Koltun, V., and Hutter, M. Learning agile and dynamic motor skills for legged robots. *Science Robotics*, 4(26):eaau5872, 2019.

Le, H., Jiang, N., Agarwal, A., Dudík, M., Yue, Y., and Daumé III, H. Hierarchical imitation and reinforcement learning. In *International conference on machine learning*, pp. 2917–2926. PMLR, 2018.

Lee, A. et al. Composing learned motor primitives for hierarchical control. In *ICLR*, 2020.

Liao, Q., Truong, T. E., Huang, X., Gao, Y., Tevet, G., Sreenath, K., and Liu, C. K. Beyondmimic: From motion tracking to versatile humanoid control via guided diffusion. *arXiv preprint arXiv:2508.08241*, 2025.

Lillicrap, T. et al. Continuous control with deep reinforcement learning. In *ICLR*, 2016.

Makoviychuk, V. et al. Isaac gym: High performance gpu-based physics simulation for robot learning. In *Proceedings of Robotics: Science and Systems (RSS)*, 2021.

Merel, J. et al. Neural probabilistic motor primitives for humanoid control. In *ICLR*, 2018.

Parisi, S., Pirotta, M., Smacchia, N., Bascetta, L., and Restelli, M. Multi-objective reinforcement learning: A comprehensive overview. *IEEE Transactions on Neural Networks and Learning Systems*, 2014.

Peng, X. B., Abbeel, P., Levine, S., and Van de Panne, M. Deepmimic: Example-guided deep reinforcement learning of physics-based character skills. *ACM Transactions On Graphics (TOG)*, 37(4):1–14, 2018.

Peng, X. B. et al. Learning agile robotic locomotion skills by imitating animals. In *Robotics: Science and Systems (RSS)*, 2020.

Peng, X. B. et al. Amp: Adversarial motion priors for stylized physics-based character control. *ACM Transactions on Graphics (TOG)*, 40(4), 2021.

Schulman, J., Moritz, P., Levine, S., Jordan, M., and Abbeel, P. High-dimensional continuous control using generalized advantage estimation. *arXiv preprint arXiv:1506.02438*, 2015.

Schulman, J., Wolski, F., Dhariwal, P., Radford, A., and Klimov, O. Proximal policy optimization algorithms. *arXiv preprint arXiv:1707.06347*, 2017a.

Schulman, J., Wolski, F., Dhariwal, P., Radford, A., and Klimov, O. Proximal policy optimization algorithms. *arXiv preprint arXiv:1707.06347*, 2017b.

Sener, O. and Koltun, V. Multi-task learning as multi-objective optimization. *Advances in neural information processing systems*, 31, 2018.

Sutton, R. S., McAllester, D., Singh, S., and Mansour, Y. Policy gradient methods for reinforcement learning with function approximation. In *Advances in Neural Information Processing Systems*, 2000.

Todorov, E. et al. Mujoco: A physics engine for model-based control. In *IROS*, 2012.

Torabi, M. et al. Behavioral cloning from observation. *arXiv preprint arXiv:1805.01905*, 2018.

Wu, Y.-H., Charoenphakdee, N., Bao, H., Tangkaratt, V., and Sugiyama, M. Imitation learning from imperfect demonstration. In *International Conference on Machine Learning*, pp. 6818–6827. PMLR, 2019.

Yu, T., Kumar, S., Gupta, A., Levine, S., Hausman, K., and Finn, C. Gradient surgery for multi-task learning. In *Advances in Neural Information Processing Systems*, 2020.

Ze, Y., Chen, Z., Araújo, J. P., Cao, Z.-a., Peng, X. B., Wu, J., and Liu, C. K. Twist: Teleoperated whole-body imitation system. *arXiv preprint arXiv:2505.02833*, 2025.

Zhan, G., Zheng, Z., and Li, S. E. Canonical form of datatic description in control systems. In *2025 American Control Conference (ACC)*, pp. 3479–3484. IEEE, 2025.

Zheng, Z. Trackerlab: One step unify isaaclab with multi-mode whole-body control., 2025a. URL https://github.com/interval-package/trackerLab.

Zheng, Z. beyondamp: One step unify isaaclab with amp., 2025b. URL https://github.com/Renforce-Dynamics/beyondAMP.

Zheng, Z., Zhan, G., Liu, S., Lyu, Y., Zhang, T., and Li, S. E. Jump-start reinforcement learning with self-evolving priors for extreme monopedal locomotion. *arXiv preprint arXiv:2507.01243*, 2025a.

Zheng, Z., Zhan, G., Shuai, B., Qin, S., Li, J., Zhang, T., and Li, S. E. Transferable latent-to-latent locomotion policy for efficient and versatile motion control of diverse legged robots. In *IEEE/RSJ International Conference on Intelligent Robots and Systems (IROS)*, 2025b.

Ziebart, B. D., Maas, A. L., Bagnell, J. A., and Dey, A. K. Maximum entropy inverse reinforcement learning. In *AAAI Conference on Artificial Intelligence*, 2008.

A. Proofs

A.1. Gradient Decomposition

Proof of Lemma 3.2. Recall that the scalarized objective is defined as

$$J_\lambda(\pi_\theta) = \lambda J_{\text{task}}(\pi_\theta) + (1-\lambda) J_{\text{style}}(\pi_\theta), \tag{25}$$

where $\lambda \in [0,1]$ is a scalar weighting coefficient.

We consider the policy gradient of J_λ with respect to the policy parameters θ. By the linearity of differentiation, the gradient of a linear combination of scalar-valued functions is equal to the same linear combination of their gradients. Therefore, we have

$$\begin{aligned} \nabla_\theta J_\lambda(\pi_\theta) &= \nabla_\theta \left(\lambda J_{\text{task}}(\pi_\theta) + (1-\lambda) J_{\text{style}}(\pi_\theta)\right) \\ &= \lambda \nabla_\theta J_{\text{task}}(\pi_\theta) + (1-\lambda) \nabla_\theta J_{\text{style}}(\pi_\theta). \end{aligned} \tag{26}$$

Defining

$$g_{\text{task}} = \nabla_\theta J_{\text{task}}(\pi_\theta), \quad g_{\text{style}} = \nabla_\theta J_{\text{style}}(\pi_\theta), \tag{27}$$

we obtain

$$\nabla_\theta J_\lambda(\pi_\theta) = \lambda g_{\text{task}} + (1-\lambda) g_{\text{style}}, \tag{28}$$

which completes the proof. □

A.2. First Order Gradient Property

Proof of Lemma 3.3. Consider a single gradient-based update of the policy parameters

$$\theta' = \theta + \eta h, \tag{29}$$

where h denotes the update direction and $\eta > 0$ is the step size.

The change in the objective J_i after this update is given by

$$\Delta J_i = J_i(\theta') - J_i(\theta) = J_i(\theta + \eta h) - J_i(\theta). \tag{30}$$

By the first-order Taylor expansion of J_i around θ, we have

$$J_i(\theta + \eta h) = J_i(\theta) + \eta \langle \nabla_\theta J_i(\theta), h \rangle + o(\eta), \tag{31}$$

where $o(\eta)$ denotes higher-order terms that vanish faster than η as $\eta \to 0$.

Substituting this expansion into the expression for ΔJ_i, we obtain

$$\Delta J_i = \eta \langle \nabla_\theta J_i(\theta), h \rangle + o(\eta). \tag{32}$$

For sufficiently small step sizes η, the leading-order term dominates the change in the objective, implying that the first-order improvement of J_i is proportional to the inner product $\langle g_i, h \rangle$, where $g_i = \nabla_\theta J_i(\theta)$. This completes the proof. □

A.3. Imitation distinguishes task-equivalent policies

Proof of Proposition 3.5. By assumption, the imitation objective $J_{\text{style}}(\pi)$ depends on the occupancy measure ρ_π. Let $\pi_1, \pi_2 \in \Pi^\star_{\text{task}}$ be such that $\rho_{\pi_1} \neq \rho_{\pi_2}$.

Since J_{style} is a functional of ρ_π, we may write

$$J_{\text{style}}(\pi) = \mathcal{F}(\rho_\pi) \tag{33}$$

for some functional $\mathcal{F}$. Unless $\mathcal{F}$ is constant over distinct occupancy measures, it follows that

$$\mathcal{F}(\rho_{\pi_1}) \neq \mathcal{F}(\rho_{\pi_2}), \tag{34}$$

which implies

$$J_{\text{style}}(\pi_1) \neq J_{\text{style}}(\pi_2). \tag{35}$$

This concludes the proof. □

A.4. Failure of linear scalarization under misalignment

Proof of Theorem 3.7. Under Assumption 3.6, for all $\pi \in \Pi^\star_{\text{task}}$,

$$J_{\text{style}}(\pi) \leq -\delta, \tag{36}$$

up to an additive constant determined by the choice of divergence.

Consider any $\lambda \in (0,1)$ and any $\pi^\star \in \Pi^\star_{\text{task}}$. For any policy $\tilde{\pi}$ such that $J_{\text{style}}(\tilde{\pi}) > J_{\text{style}}(\pi^\star)$, we have

$$J_\lambda(\tilde{\pi}) - J_\lambda(\pi^\star) = \lambda\big(J_{\text{task}}(\tilde{\pi}) - J_{\text{task}}(\pi^\star)\big) + (1-\lambda)\big(J_{\text{style}}(\tilde{\pi}) - J_{\text{style}}(\pi^\star)\big). \tag{37}$$

Since $J_{\text{task}}(\pi^\star)$ is maximal, the first term is non-positive. However, the second term is strictly positive by construction. Therefore, for sufficiently large improvement in J_{style}, the scalarized objective J_λ is strictly larger at $\tilde{\pi}$ than at $\pi^\star$.

Hence, no task-optimal policy can be a maximizer of J_λ for $\lambda < 1$, which completes the proof. □

A.5. Closed-form solution

Proof of Proposition 3.8. We consider the constrained optimization problem

$$\max_{\Delta\theta} \ \langle g_{\text{style}}, \Delta\theta\rangle \quad \text{s.t.} \quad \langle g_{\text{task}}, \Delta\theta\rangle \geq 0, \ \ \|\Delta\theta\|_2 \leq \epsilon. \tag{38}$$

Since the objective is linear and the feasible set is convex, this problem is convex and satisfies Slater's condition. Therefore, strong duality holds and the Karush–Kuhn–Tucker (KKT) conditions are necessary and sufficient for optimality.

The Lagrangian is given by

$$\mathcal{L}(\Delta\theta, \lambda, \mu) = -\langle g_{\text{style}}, \Delta\theta\rangle + \lambda\big(-\langle g_{\text{task}}, \Delta\theta\rangle\big) + \mu\big(\|\Delta\theta\|_2^2 - \epsilon^2\big), \tag{39}$$

where $\lambda \geq 0$ and $\mu \geq 0$ are the dual variables associated with the task-feasibility constraint and the trust-region constraint, respectively.

Taking the derivative of the Lagrangian with respect to $\Delta\theta$ and setting it to zero yields the stationarity condition

$$-g_{\text{style}} - \lambda g_{\text{task}} + 2\mu\Delta\theta = 0, \tag{40}$$

which implies

$$\Delta\theta = \frac{1}{2\mu}\big(g_{\text{style}} + \lambda g_{\text{task}}\big). \tag{41}$$

If the task-feasibility constraint is inactive ($\lambda = 0$), the solution reduces to normalized imitation-gradient ascent. Otherwise, when the constraint is active ($\lambda > 0$), complementary slackness implies

$$\langle g_{\text{task}}, \Delta\theta\rangle = 0. \tag{42}$$

Substituting the expression for $\Delta\theta$ into the above condition yields

$$\langle g_{\text{task}}, g_{\text{style}} + \lambda g_{\text{task}}\rangle = 0. \tag{43}$$

The trust-region constraint $\|\Delta\theta\|_2 \leq \epsilon$ only affects the magnitude of the update. Hence, the optimal solution is fully characterized by its direction, which lies in the two-dimensional subspace spanned by $\{g_{\text{task}}, g_{\text{style}}\}$. We therefore represent the update direction as

$$g^* = \alpha g_{\text{task}} + (1-\alpha) g_{\text{style}}, \qquad \alpha \in \mathbb{R}. \tag{44}$$

Imposing the active task-feasibility constraint $\langle g_{\text{task}}, g^*\rangle = 0$ yields

$$\alpha\|g_{\text{task}}\|_2^2 + (1-\alpha)\langle g_{\text{task}}, g_{\text{style}}\rangle = 0, \tag{45}$$

which admits the unique solution

$$\alpha = \frac{\langle g_{\text{task}}, g_{\text{task}} - g_{\text{style}} \rangle}{\|g_{\text{task}} - g_{\text{style}}\|_2^2}. \tag{46}$$

Finally, since the update direction must remain a convex combination of g_{task} and g_{style} to preserve feasibility, the coefficient α is clipped to the interval $[0, 1]$:

$$\alpha = \text{clip}\left(\frac{\langle g_{\text{task}}, g_{\text{task}} - g_{\text{style}} \rangle}{\|g_{\text{task}} - g_{\text{style}}\|_2^2},\ 0,\ 1 \right). \tag{47}$$

This completes the proof. □

A.6. Feasibility of Projected Update

Proof of Lemma 3.12. Recall that the TCMP update direction is defined as

$$g^* = g_{\text{task}} + \beta\, \Pi_{\perp g_{\text{task}}}(g_{\text{style}}), \qquad \beta \geq 0, \tag{48}$$

where $\Pi_{\perp g_{\text{task}}}(\cdot)$ denotes the orthogonal projection onto the subspace perpendicular to g_{task}, i.e.,

$$\Pi_{\perp g_{\text{task}}}(g_{\text{style}}) = g_{\text{style}} - \frac{\langle g_{\text{style}}, g_{\text{task}} \rangle}{\|g_{\text{task}}\|_2^2} g_{\text{task}}. \tag{49}$$

By construction, the projected component is orthogonal to g_{task}. Indeed,

$$\begin{aligned} \langle g_{\text{task}}, \Pi_{\perp g_{\text{task}}}(g_{\text{style}}) \rangle &= \langle g_{\text{task}}, g_{\text{style}} \rangle - \frac{\langle g_{\text{style}}, g_{\text{task}} \rangle}{\|g_{\text{task}}\|_2^2} \langle g_{\text{task}}, g_{\text{task}} \rangle \\ &= \langle g_{\text{task}}, g_{\text{style}} \rangle - \langle g_{\text{task}}, g_{\text{style}} \rangle \\ &= 0. \end{aligned} \tag{50}$$

We now evaluate the inner product between the task gradient and the TCMP update:

$$\begin{aligned} \langle g_{\text{task}}, g^* \rangle &= \langle g_{\text{task}}, g_{\text{task}} + \beta\, \Pi_{\perp g_{\text{task}}}(g_{\text{style}}) \rangle \\ &= \|g_{\text{task}}\|_2^2 + \beta\, \langle g_{\text{task}}, \Pi_{\perp g_{\text{task}}}(g_{\text{style}}) \rangle. \end{aligned} \tag{51}$$

Using Eq. (50), the second term vanishes, yielding

$$\langle g_{\text{task}}, g^* \rangle = \|g_{\text{task}}\|_2^2 \ \geq\ 0. \tag{52}$$

Therefore, the TCMP update direction g^* is task-feasible in the sense that it does not decrease the task objective to first order. □ □

A.7. Task-Feasible Descent

Proof of Theorem 3.13. We prove that the TCMP update yields a non-decreasing task objective up to first-order approximation.

Recall that the task objective $J_{\text{task}}(\theta)$ is assumed to be continuously differentiable and L-smooth with respect to θ (Assumption 3.10). By the first-order Taylor expansion, for any update direction g and step size $\eta > 0$, we have

$$J_{\text{task}}(\theta + \eta g) = J_{\text{task}}(\theta) + \eta\, \langle \nabla_\theta J_{\text{task}}(\theta), g \rangle + \mathcal{O}(\eta^2). \tag{53}$$

In our setting, the update direction is given by the TCMP rule g^* defined in Eq. (14). By Lemma 3.12, g^* is task-feasible, i.e.,

$$\langle \nabla_\theta J_{\text{task}}(\theta), g^* \rangle = \langle g_{\text{task}}, g^* \rangle \geq 0. \tag{54}$$

Substituting $g = g^*$ into Eq. (53) yields

$$J_{\text{task}}(\theta + \eta g^*) \geq J_{\text{task}}(\theta) + \eta \langle g_{\text{task}}, g^* \rangle - \mathcal{O}(\eta^2). \tag{55}$$

Since $\langle g_{\text{task}}, g^* \rangle \geq 0$ and the higher-order remainder term is bounded by smoothness, there exists a sufficiently small step size $\eta > 0$ such that

$$J_{\text{task}}(\theta + \eta g^*) \geq J_{\text{task}}(\theta), \tag{56}$$

which proves the claim. □

□

A.8. Characterization of Task-Priority Stationarity

Proof of Lemma 3.16. We prove the statement by establishing both directions.

(⇒) Necessity. Assume that $\theta^\star$ is task-priority stationary, i.e., the TCMP update direction vanishes at $\theta^\star$:

$$g^*(\theta^\star) = 0. \tag{57}$$

We consider two cases.

Case 1: $g_{task}(\theta^\star) = 0$. In this case, $\theta^\star$ is a stationary point of the task objective, and the condition in the lemma holds trivially.

Case 2: $g_{task}(\theta^\star) \neq 0$. Recall that the TCMP update direction is given by

$$g^* = g_{\text{task}} + \beta \, \Pi_{\perp g_{\text{task}}}(g_{\text{style}}), \qquad \beta \geq 0, \tag{58}$$

where $\Pi_{\perp g_{\text{task}}}(\cdot)$ denotes the orthogonal projection onto the subspace perpendicular to g_{task}.

Since $g_{\text{task}}(\theta^\star) \neq 0$ and $g^*(\theta^\star) = 0$, the projected imitation component must exactly cancel the task gradient. However, by construction, $\Pi_{\perp g_{\text{task}}}(g_{\text{style}})$ is orthogonal to g_{task}. Therefore, the only way for Eq. (58) to vanish is

$$\Pi_{\perp g_{\text{task}}}(g_{\text{style}}(\theta^\star)) = 0. \tag{59}$$

Eq. (59) implies that $g_{\text{style}}(\theta^\star)$ lies in the span of $g_{\text{task}}(\theta^\star)$, i.e.,

$$g_{\text{style}}(\theta^\star) = c \, g_{\text{task}}(\theta^\star) \quad \text{for some } c \in \mathbb{R}. \tag{60}$$

Since $\beta \geq 0$ and $g^*(\theta^\star) = 0$, substituting Eq. (60) into Eq. (58) yields

$$g_{\text{task}}(\theta^\star) + \beta \, c \, g_{\text{task}}(\theta^\star) = 0, \tag{61}$$

which requires $1 + \beta c = 0$. Because $\beta \geq 0$, this equality is possible only when $c \leq 0$. Equivalently,

$$\langle g_{\text{task}}(\theta^\star), g_{\text{style}}(\theta^\star) \rangle = c \, \|g_{\text{task}}(\theta^\star)\|_2^2 \leq 0. \tag{62}$$

This completes the proof of necessity.

(⇐) Sufficiency. We now prove the converse.

If $g_{\text{task}}(\theta^\star) = 0$, then by definition the TCMP update direction vanishes, and $\theta^\star$ is task-priority stationary.

Otherwise, assume $g_{\text{task}}(\theta^\star) \neq 0$ and

$$\langle g_{\text{task}}(\theta^\star), g_{\text{style}}(\theta^\star) \rangle \leq 0. \tag{63}$$

Under this condition, the constrained optimization defining TCMP (Eq. (14)) admits the trivial solution $g^*(\theta^\star) = 0$ as its minimizer, since any nonzero update direction would either violate task feasibility or increase the update norm. Consequently, the TCMP update direction vanishes at $\theta^\star$, and $\theta^\star$ is task-priority stationary. □

A.9. Limit Point Optimality of TCMP

Proof of Theorem 3.17. Let $\{\theta_k\}$ be the sequence generated by TCMP, and suppose that it admits a limit point $\theta^\star$. By definition of limit point, there exists a subsequence $\{\theta_{k_j}\}$ such that $\theta_{k_j} \to \theta^\star$ as $j \to \infty$.

We proceed by contradiction. Assume that $\theta^\star$ is not task-priority stationary. Then, by Def. 3.15, there exists a direction $h \in \mathcal{C}_{\text{task}}(\theta^\star)$ such that

$$\langle g_{\text{task}}(\theta^\star), h\rangle > 0. \tag{64}$$

By continuity of the gradients (Assumption 3.10), there exists a neighborhood $\mathcal{U}$ of $\theta^\star$ such that for all $\theta \in \mathcal{U}$,

$$\langle g_{\text{task}}(\theta), h\rangle > 0. \tag{65}$$

In particular, for sufficiently large j, $\theta_{k_j} \in \mathcal{U}$.

During iteration k_j, TCMP computes the update direction $g^*(\theta_{k_j})$ as the solution to the task-feasible projection defined in Eq. (14). By construction, $g^*(\theta_{k_j})$ maximizes $\langle g_{\text{task}}(\theta_{k_j}), h\rangle$ over all task-feasible directions. Since h is task-feasible and yields a strictly positive inner product, it follows that

$$\langle g_{\text{task}}(\theta_{k_j}), g^*(\theta_{k_j})\rangle \geq \langle g_{\text{task}}(\theta_{k_j}), h\rangle > 0. \tag{66}$$

By the task-feasible descent guarantee (Theorem 3.13), there exists $\epsilon > 0$ such that for all sufficiently small step sizes,

$$J_{\text{task}}(\theta_{k_j+1}) > J_{\text{task}}(\theta_{k_j}), \tag{67}$$

which contradicts the assumption that $\theta^\star$ is a limit point of the sequence $\{\theta_k\}$.

Therefore, $\theta^\star$ must be task-priority stationary. □

A.10. Convergence of TCMP

Proof of Theorem 3.19. We prove that the sequence $\{\theta_k\}$ generated by TCMP converges to a task-priority stationary point.

Step 1: Monotonicity of the task objective. By Theorem 3.13, under Assumption 3.10 and for a step size η_k satisfying Assumption 3.18, the TCMP update

$$\theta_{k+1} = \theta_k + \eta_k g^*(\theta_k) \tag{68}$$

ensures

$$J_{\text{task}}(\theta_{k+1}) \geq J_{\text{task}}(\theta_k) \tag{69}$$

up to first-order approximation. Hence, $\{J_{\text{task}}(\theta_k)\}$ is a non-decreasing sequence.

Step 2: Boundedness and convergence of objective values. Under Assumption 3.10, the task objective $J_{\text{task}}(\theta)$ is upper bounded. Therefore, the monotone sequence $\{J_{\text{task}}(\theta_k)\}$ converges to a finite limit:

$$\lim_{k\to\infty} J_{\text{task}}(\theta_k) = J^\star. \tag{70}$$

Step 3: Vanishing update directions. Suppose, by contradiction, that there exists an $\varepsilon > 0$ and an infinite subsequence $\{k_j\}$ such that

$$\|g^*(\theta_{k_j})\|_2 \geq \varepsilon. \tag{71}$$

By the Lipschitz continuity of ∇J_{task} (Assumption 3.10), there exists a constant $c > 0$ such that each TCMP update with sufficiently small step size satisfies

$$J_{\text{task}}(\theta_{k_j+1}) \geq J_{\text{task}}(\theta_{k_j}) + c\,\eta_{k_j}\|g^*(\theta_{k_j})\|_2^2. \tag{72}$$

Combining Eqs. (71) and (72) yields a strictly positive improvement lower bound along the subsequence:

$$J_{\text{task}}(\theta_{k_j+1}) - J_{\text{task}}(\theta_{k_j}) \geq c\,\eta_{k_j}\varepsilon^2. \tag{73}$$

Summing over j leads to an unbounded increase of $J_{\text{task}}(\theta_k)$, contradicting the convergence in Eq. (70). Therefore,

$$\lim_{k\to\infty} \|g^*(\theta_k)\|_2 = 0. \tag{74}$$

Step 4: Characterization of limit points. Let $\theta^\star$ be any accumulation point of $\{\theta_k\}$. By continuity of $g^*(\cdot)$ and Eq. (74), we have

$$g^*(\theta^\star) = 0. \tag{75}$$

By Lemma 3.16, $\theta^\star$ is a task-priority stationary point as defined in Def. 3.15.

Conclusion. Since every accumulation point of $\{\theta_k\}$ is task-priority stationary, the TCMP iterates converge to a task-priority stationary point. □

A.11. Reduction Property

Proof of Proposition 3.20. We analyze the two extreme geometric configurations of the task and imitation gradients.

Case 1: Conflicting gradients (reduction to PPO). Assume that the imitation gradient always conflicts with the task gradient, i.e.,

$$\langle g_{\text{task}}, g_{\text{style}} \rangle \leq 0. \tag{76}$$

Consider the TCMP mixing problem

$$\min_{\alpha \in [0,1]} \left\| \alpha g_{\text{task}} + (1-\alpha) g_{\text{style}} \right\|_2^2. \tag{77}$$

Expanding the squared norm yields

$$\begin{aligned} \|\alpha g_{\text{task}} + (1-\alpha) g_{\text{style}}\|_2^2 = \alpha^2 \|g_{\text{task}}\|_2^2 + (1-\alpha)^2 \|g_{\text{style}}\|_2^2 \\ + 2\alpha(1-\alpha)\langle g_{\text{task}}, g_{\text{style}} \rangle. \end{aligned} \tag{78}$$

Under condition (76), the cross term is non-positive, and the objective is minimized at the boundary $\alpha = 1$. Therefore,

$$g^* = g_{\text{task}}, \tag{79}$$

which coincides with the standard PPO update direction. Hence, TCMP reduces to PPO in the presence of persistent gradient conflict.

Case 2: Aligned gradients (reduction to Adversarial Imitation-style update). Now suppose the gradients are locally aligned, i.e.,

$$\langle g_{\text{task}}, g_{\text{style}} \rangle > 0. \tag{80}$$

In this case, the minimizer of (77) lies in the interior of the interval $(0, 1)$ whenever the gradient magnitudes are comparable. Consequently,

$$g^* = \alpha g_{\text{task}} + (1-\alpha) g_{\text{style}}, \qquad \alpha \in (0, 1), \tag{81}$$

which is a convex combination of the task and imitation gradients.

This update direction is equivalent to an adversarial imitation-style policy update, where task and imitation signals jointly influence the policy gradient.

Conclusion. TCMP interpolates between pure task optimization and reward-mixed adversarial imitation learning, reducing to PPO under gradient conflict and recovering adversarial imitation-style updates when the gradients are locally aligned.

□

B. Environments

This appendix provides the simulation environment specifications for the eight tasks used in our experiments (B.1–B.8). All tasks are implemented in Isaac Lab and simulated with PhysX. Unless otherwise stated, each environment runs 4096 parallel instances with environment spacing 2.5 m, uses a physics time step of $\Delta t = 0.005s$, and applies actions at 50 Hz

Table 3. Detailed reward terms and weights.

	Reward Terms					
Category	**Reward**	**Equation**	**W**	**Reward**	**Equation**	**W**
Task terms						
Velocity tracking	$R_{\text{track\_lin\_vel}}$	$\exp\left(-\frac{\|\min(v,v^{\text{cmd}})-v^{\text{cmd}}\|^2}{0.25}\right)$	1.5	$R_{\text{track\_ang\_vel}}$	$\exp\left(-\frac{(\omega_{\text{yaw}}-\omega_{\text{yaw}}^{\text{cmd}})^2}{0.25}\right)$	0.5
Task completion	$R_{\text{termination}}$	Termination	-200	$R_{\text{out\_bound}}$	Reach terrain bound	200
Dense terms						
Platform constraint	$R_{\text{out\_platform}}$	$\mathbf{1}\{\|x\|>3\}$	10.0	$R_{\text{reach\_far}}$	$\exp(-\|x\|)$	-0.5
Posture terms						
Vertical stability	R_{v_z}	v_z^2	-0.5	$R_{\omega_{xy}}$	$\|\omega_{xy}\|^2$	-0.05
Orientation	$R_{\text{orientation}}$	$\|g-g_{\text{target}}\|^2$	-1.0	–	–	–
Smoothness and contact terms						
Energy	$R_{\text{joint\_torques}}$	$\sum_j \tau_j^2$	-1.0×10^{-5}	$R_{\text{joint\_power}}$	$\sum_j \|\tau_j\dot{q}_j\|$	-2.0×10^{-5}
Action smoothness	$R_{\text{action\_rate}}$	$\sum_j(a_t-a_{t-1})^2$	-0.01	$R_{\text{action\_smoothness}}$	$\sum_j(a_t-2a_{t-1}+a_{t-2})^2$	-0.01
Regularization	$R_{\text{joint\_acc}}$	$\sum_j \ddot{q}_j^2$	-2.5×10^{-7}	$R_{\text{joint\_deviation}}$	$\sum_j(q_j-q_j^{\text{default}})^2$	-0.01
Contact safety	$R_{\text{collision}}$	$\sum_i \mathbf{1}\{F_i>0.1\}$	-10.0	R_{stumble}	$\mathbf{1}\{\exists i, \|F_i^{xy}\|>4\|F_i^z\|\}$	-1.0
Edge contact	$R_{\text{feet\_edge}}$	$\sum_i c_i \sum_d \omega_d E_d[p_i]$	-1.0	–	–	–

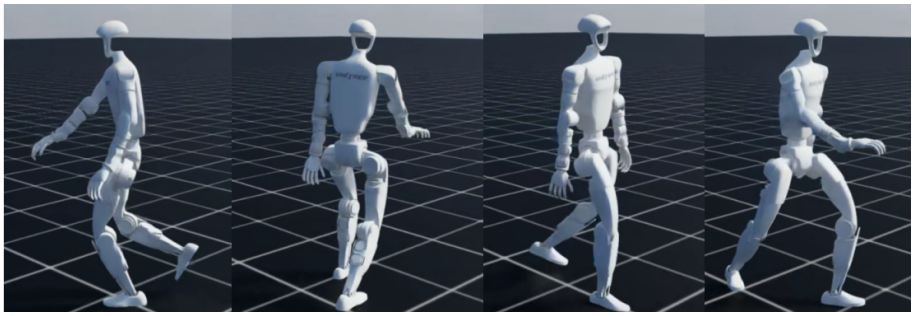

Figure 6. Natural locomotion tasks. The robot performs navigation and velocity tracking with a natural walking gait under minimal motion priors.

via a decimation factor of 4. The robot is the Unitree G1 humanoid (cylinder-collision variant). The control interface is a joint-space position target interface (PD position control internally in Isaac Lab).

Below, for each task we describe its goal, command (if any), observation/action specification, reward terms (with weights), termination conditions, and key randomization settings.

Appendix B: Task Environments

This appendix summarizes the task environments used in our experiments. Tasks are grouped into four families according to their control objectives and motion priors: (i) natural locomotion, (ii) punching and motion imitation, (iii) style-specific velocity tracking with dog-like gait, and (iv) style-specific velocity tracking with knee-walking gait.

B.1. B.1 Natural Locomotion Tasks

Purpose. This task family evaluates command-conditioned locomotion with minimal motion priors, focusing on general-purpose velocity tracking and navigation behaviors.

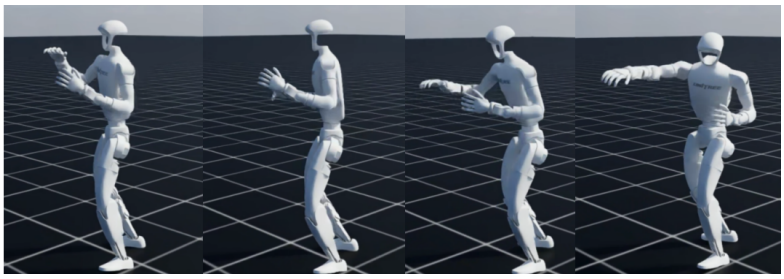

Figure 7. Punching and motion-imitation tasks. These tasks evaluate whole-body motion generation under imitation objectives and task-conditioned striking commands.

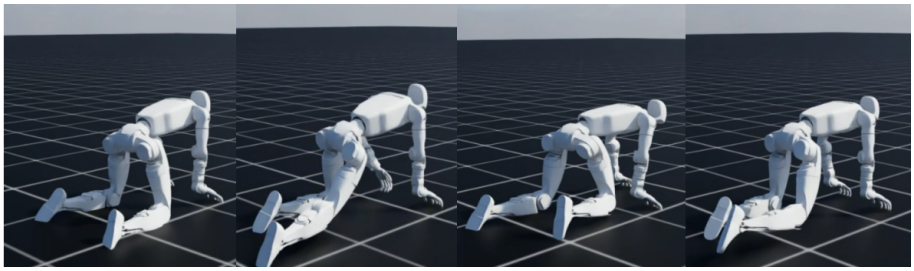

Figure 8. Style-specific velocity tracking with dog-like gait. The robot tracks commanded velocities while following a non-human locomotion style.

B.1.1 Velocity (Natural) The robot tracks commanded planar linear and angular velocities while maintaining a natural walking gait on flat terrain. Performance is evaluated based on velocity tracking accuracy and locomotion stability.

B.1.2 Navigation (E2E) The robot navigates toward a randomly sampled planar goal pose by generating end-to-end whole-body locomotion. The task evaluates goal-reaching accuracy and stable orientation alignment.

B.2. B.2 Punching and Motion-Imitation Tasks

Purpose. This task family evaluates whole-body motion generation under strong motion priors, ranging from pure imitation to task-driven striking behaviors.

B.2.1 Punch (AMP-only) The robot generates stable full-body punching motions without an explicit task-level objective, serving as a pure motion-style optimization setting.

B.2.2 Punch (Hit-task) The robot performs command-conditioned punching, where successful strikes are explicitly rewarded. This task evaluates task-driven control under strong motion-style constraints.

B.2.3 Tracking The robot tracks a commanded whole-body reference motion defined by anchor- and body-level kinematic targets. The task evaluates motion imitation accuracy and balance maintenance.

B.2.4 Tracking (PHC) Tracking (PHC) extends the standard Tracking task by progressively increasing command difficulty via a curriculum schedule with not on trajectory reset, evaluating robustness under expanding motion perturbations.

B.3. B.3 Style-Specific Velocity Tasks: DogMove

Purpose. This task evaluates velocity tracking performance under a dog-like locomotion style induced by motion priors.

B.4. B.4 Style-Specific Velocity Tasks: KneeWalk

Purpose. This task evaluates velocity tracking under a knee-walking locomotion style, testing robustness under alternative contact and support patterns.

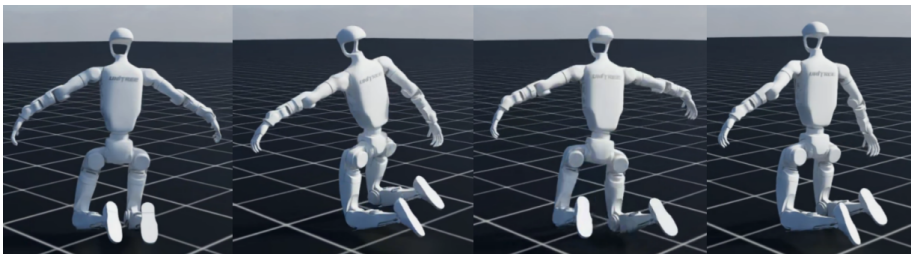

Figure 9. Style-specific velocity tracking with knee-walking gait. The robot performs command-conditioned locomotion under alternative contact patterns.

Table 4. Core hyper-parameters of TCMP.

Category	Hyper-parameters	Value
Base (PPO)	Optimizer	Adam
	Learning rate	1.0×10^{-3}
	Learning rate schedule	Adaptive (target KL = 0.01)
	Discount factor (γ)	0.99
	GAE parameter (λ)	0.95
	PPO clip range (ϵ)	0.2
	Entropy coefficient	0.005
	Value loss coefficient	1.0
	Clipped value loss	True
	Max gradient norm	1.0
	Steps per env per iteration	24
	Number of iterations	3000 (most tasks) / 10000 (natural velocity)
Networks	Policy network	3-layer MLP, hidden dims [512, 256, 128], ELU
	Value network	3-layer MLP, hidden dims [512, 256, 128], ELU
	Discriminator network	2-layer MLP, hidden dims [256, 256], ReLU
	Initial action noise std	1.0
TCMP (Style module)	Style reward coefficient (c_{style})	0.5
	Style replay buffer size	100000
	Gradient penalty coefficient (λ_{gp})	10
	Discriminator weight decay	trunk: 10^{-3}, head: 10^{-1}
	Discriminator loss	MSE (expert: +1, policy: -1)

C. Implementation Details

C.1. Training stabilization

For training efficiency, we only calculate the alpha once each iteration and after that we use that alpha for target object linear scalarization.

C.2. Hyperparameters

The hyper-parameter settings are listed in Table 4.

D. Additional Experiment Results

D.1. Training Curves

This subsection presents the training dynamics of individual reward components across all evaluated tasks. For each task, we separately report the evolution of the AMP (imitation-based) reward, smoothness regularization reward, and task-specific reward throughout training.

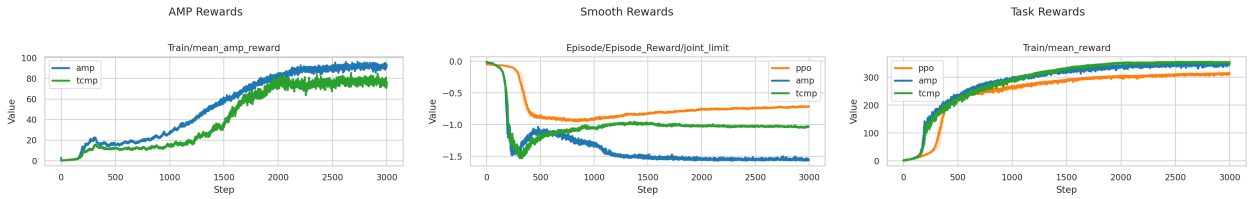

(a) Velocity (DogMove) – AMP Reward *(b)* Velocity (DogMove) – Smooth Reward *(c)* Velocity (DogMove) – Task Reward

Figure 10. Training curves of individual reward components for the DogMove velocity tracking task. From left to right, the plots show the AMP (imitation) reward, smoothness regularization reward, and task-specific velocity reward, respectively. The curves illustrate the evolution and interaction of different objectives during training.

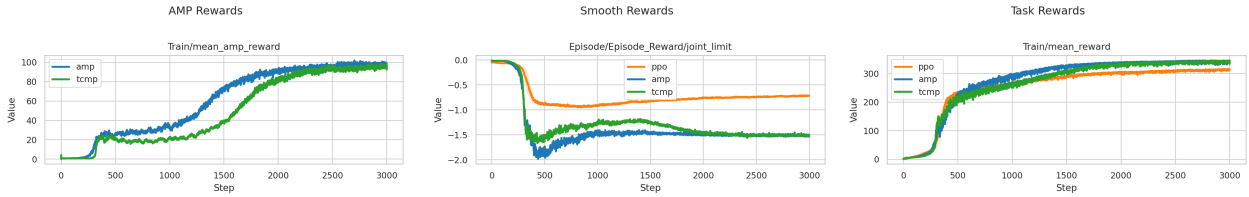

(a) Velocity (KneeWalk) – AMP Reward *(b)* Velocity (KneeWalk) – Smooth Reward *(c)* Velocity (KneeWalk) – Task Reward

Figure 11. Training curves of individual reward components for the KneeWalk velocity tracking task. From left to right, the plots report the AMP reward, smoothness regularization reward, and task-specific velocity reward. These results provide insight into how imitation and task objectives are balanced under altered locomotion constraints.

The purpose of these curves is twofold. First, they provide a fine-grained view of the optimization process that is not visible from final performance metrics alone. Second, they help illustrate how different reward components interact under varying task definitions, demonstration qualities, and auxiliary constraints.

These effects are especially evident in tasks with strong task constraints, modified dynamics, or distributional shifts between demonstrations and the target task, such as KneeWalk locomotion, navigation, and punch tasks with explicit hit objectives. Conversely, in settings where imitation is the primary or sole supervision signal (e.g., AMP-only punch), the training curves reflect more consistent alignment between reward components.

D.2. Performance Radar Figures

To provide a holistic comparison beyond scalar metrics, we visualize policy performance using radar plots for each task. Each radar figure compares **PPO**, **AMP**, and **TCMP** across six complementary dimensions that reflect task performance, motion quality, optimization behavior, and robustness to demonstration misalignment.

Specifically, the six axes correspond to: (1) **Task Reward**, measuring task-centric performance; (2) **Action Smoothness**, reflecting motion regularity and physical plausibility; (3) **Style Alignment**, indicating similarity to the demonstration distribution; (4) **Policy Robustness**, measuring the ability to retain useful motion priors under misaligned demonstrations; (5) **Task-Feasible Gradient**, capturing the degree to which policy updates remain compatible with task optimization; and (6) **Convergence Stability**, reflecting training stability and consistency across random seeds. All axes are normalized to $[0, 1]$ within each task to enable fair relative comparison.

Fig. 18 reports radar plots for all eight evaluated tasks.

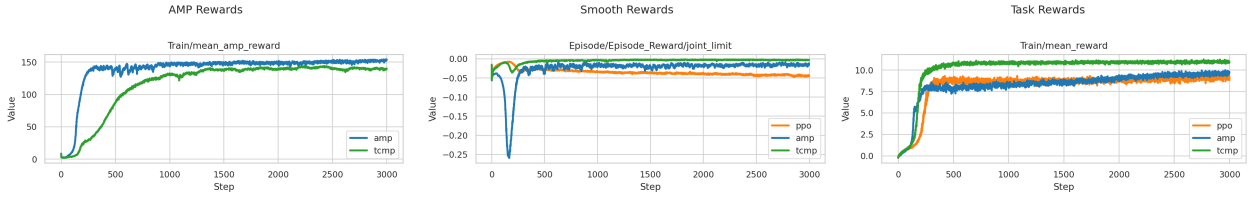

(a) Navigation (E2E) – AMP Reward *(b)* Navigation (E2E) – Smooth Reward *(c)* Navigation (E2E) – Task Reward

Figure 12. Training curves of individual reward components for the end-to-end navigation task. Columns correspond to the AMP reward, smoothness reward, and navigation task reward, respectively. The curves reveal the optimization dynamics when imitation signals are combined with long-horizon task objectives.

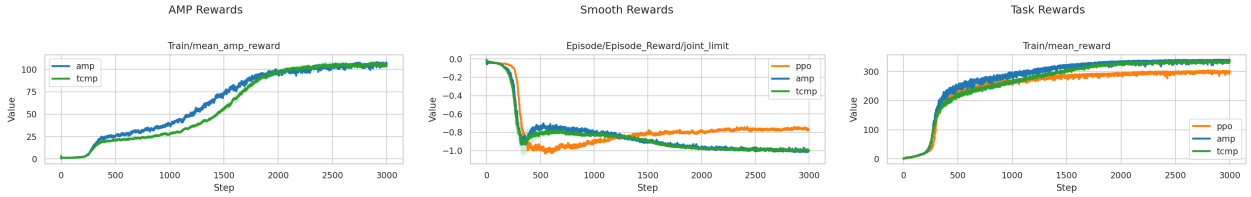

(a) Velocity (Natural) – AMP Reward *(b)* Velocity (Natural) – Smooth Reward *(c)* Velocity (Natural) – Task Reward

Figure 13. Training curves of individual reward components for the natural velocity tracking task. From left to right, the plots show the AMP reward, smoothness regularization reward, and task-specific velocity reward. This task emphasizes natural motion characteristics and highlights their interaction with task-oriented optimization.

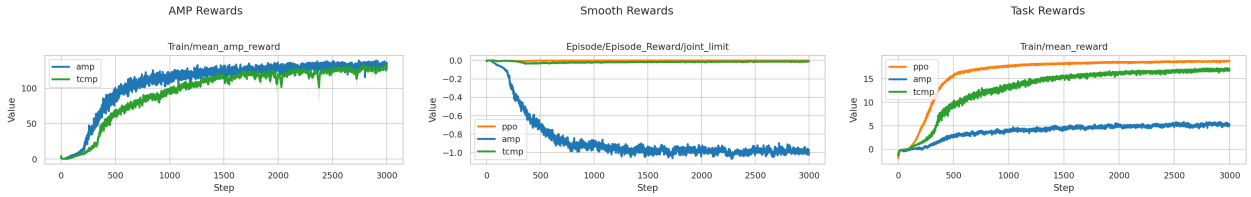

(a) Punch (AMP-only) – AMP Reward *(b)* Punch (AMP-only) – Smooth Reward *(c)* Punch (AMP-only) – Task Reward

Figure 14. Training curves of individual reward components for the Punch task trained with AMP-only supervision. From left to right, the plots show the AMP reward, smoothness reward, and task reward. This setting isolates the effect of imitation-based objectives in the absence of explicit task-driven supervision.

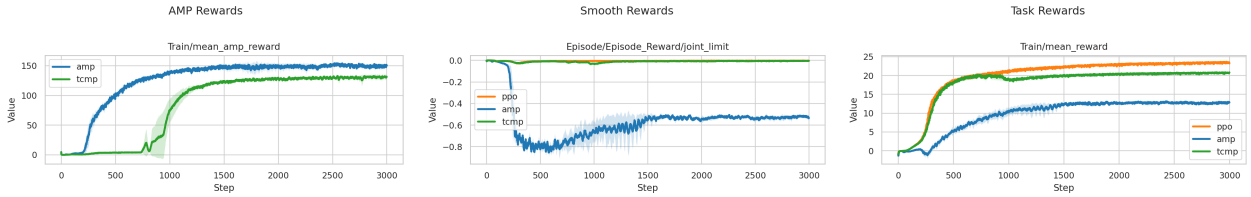

(a) Punch (Hit-task) – AMP Reward *(b)* Punch (Hit-task) – Smooth Reward *(c)* Punch (Hit-task) – Task Reward

Figure 15. Training curves of individual reward components for the Punch task with an explicit hit objective. Columns correspond to the AMP reward, smoothness regularization reward, and hit-specific task reward. The curves illustrate how task-oriented incentives interact with imitation-driven motion priors.

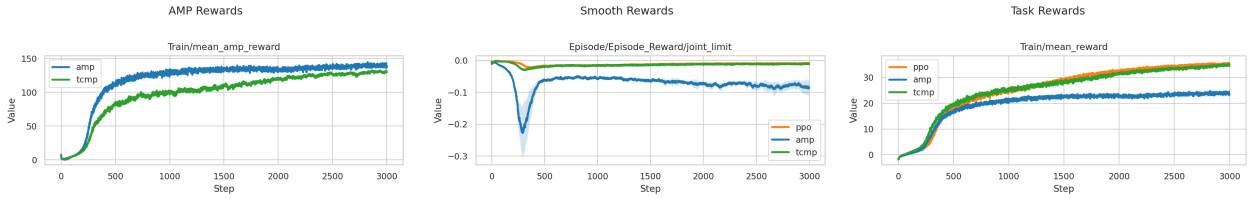

(a) Tracking – AMP Reward *(b)* Tracking – Smooth Reward *(c)* Tracking – Task Reward

Figure 16. Training curves of individual reward components for the tracking task. From left to right, the plots show the AMP reward, smoothness regularization reward, and task-specific tracking reward. These results reflect the learning dynamics under trajectory-following objectives.

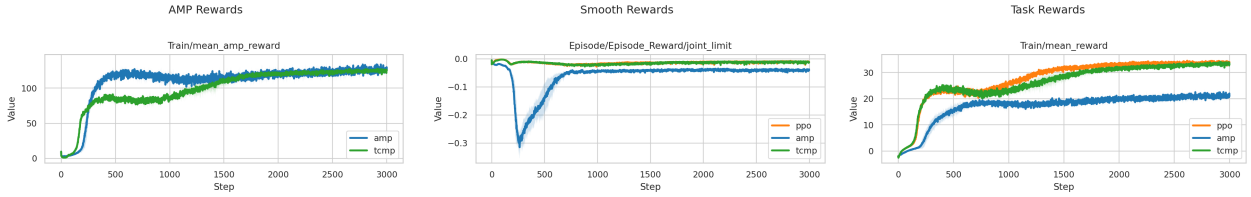

(a) Tracking (incl. PHC) – AMP Reward *(b)* Tracking (incl. PHC) – Smooth Reward *(c)* Tracking (incl. PHC) – Task Reward

Figure 17. Training curves of individual reward components for the tracking task with additional PHC constraints. From left to right, the plots report the AMP reward, smoothness reward, and task-specific tracking reward. This figure highlights the effect of auxiliary constraints on the optimization of different reward components.

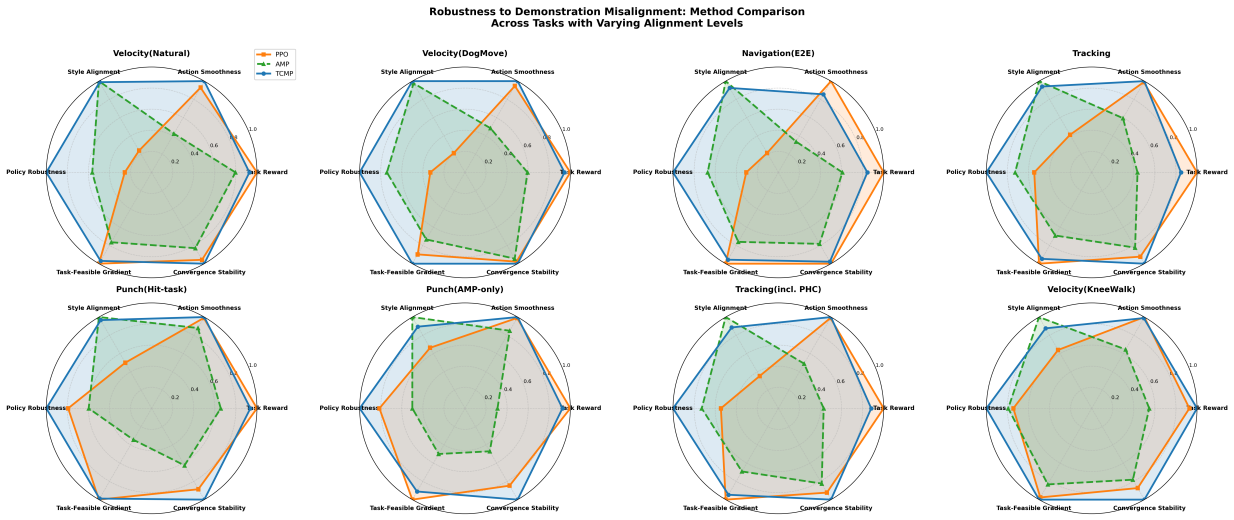

Figure 18. Radar comparison across all tasks. Each subfigure corresponds to one task and compares PPO, AMP, and TCMP across six normalized dimensions: task reward, action smoothness, style alignment, policy robustness, task-feasible gradient, and convergence stability.